Cerebral Cortex, February 2021;31: 785–794

doi: 10.1093/cercor/bhaa257
Advance Access Publication Date: 16 September 2020
Original Article

ORIGINAL ARTICLE

Contextual Fear Memory Retrieval Is Vulnerable to Hippocampal Noise

Satoshi Iwasaki[1] and Yuji Ikegaya[1,2]

[1]Graduate School of Pharmaceutical Sciences, The University of Tokyo, Tokyo 113-0033, Japan and [2]Center for Information and Neural Networks, National Institute of Information and Communications Technology, Suita City, Osaka 565-0871, Japan

Address correspondence to Yuji Ikegaya, Laboratory of Chemical Pharmacology, Graduate School of Pharmaceutical Sciences, The University of Tokyo, 7-3-1 Hongo, Bunkyo-ku, Tokyo 113-0033, Japan. Email: yuji@ikegaya.jp.

Abstract

Memory retrieval depends on reactivation of memory engram cells. Inadvertent activation of these cells is expected to cause memory-retrieval failure, but little is known about how noisy activity of memory-irrelevant neurons impacts mnemonic processes. Here, we report that optogenetic nonselective activation of only tens of hippocampal CA1 cells (~0.01% of the total cells in the CA1 pyramidal cell layer) impairs contextual fear memory recall. Memory recall failure was associated with altered neuronal reactivation in the basolateral amygdala. These results indicate that hippocampal memory retrieval requires strictly regulated activation of a specific neuron ensemble and is easily disrupted by the introduction of noisy CA1 activity, suggesting that reactivating memory engram cells as well as silencing memory-irrelevant neurons are both crucial for memory retrieval.

Key words: amygdala, Arc, hippocampus, memory, optogenetics

Introduction

Memories are experimentally identified by biologically active markers, such as immediate early genes (IEGs), for example, c-Fos and Arc, in specific neuron ensembles (Nonaka et al. 2014; Tonegawa et al. 2015). Optogenetic and chemogenetic approaches have revealed that memories are disrupted by inactivation of IEG-expressing cell ensembles during memory encoding in the hippocampus (Denny et al. 2014; Tanaka et al. 2014), amygdala (Han et al. 2009), and neocortex (Cowansage et al. 2014; Kitamura et al. 2017). Optogenetic silencing of c-Fos-positive CA1 neuron ensembles that were activated during memory acquisition prevents reactivation of the c-Fos-positive cell ensembles in not only the hippocampus but also the neocortex and disrupts contextual memory retrieval (Tanaka et al. 2014), suggesting that temporally and spatially coordinated reactivation of CA1 neurons is essential for reinstating memory traces across brain regions. Moreover, optogenetic reactivation of IEG-positive cells alone can induce memory retrieval (Liu et al. 2012). Therefore, memory retrieval depends on reactivation of IEG-positive cells.

It remains unknown how activation of IEG-negative cells, that is, nonmemory engram cells, during memory retrieval affects performance. Previous studies have demonstrated that the overlapping ratio of IEG-positive ensembles that were activated during memory encoding and memory retrieval is positively correlated with memory-retrieval performance (Reijmers et al. 2007; Tanaka et al. 2014). We thus reasoned that nonspecific cell activation disrupts memory retrieval. Consistent with this idea, an increased fraction of hyperactive CA1 neurons is observed in early Alzheimer's disease (AD) model mice, and this noisy activity may cause cognitive dysfunction (Busche et al. 2012). However, the impact of random activation of CA1 neurons on cognitive behavior or neuronal activity in the hippocampus or other brain regions has not been fully clarified. In the present study, we optogenetically manipulated a small fraction of nonspecific neurons and discovered that the surprisingly sparse nonselec-

tive activation of CA1 neurons could disrupt contextual memory retrieval and alter active cell ensembles in the amygdala.

Materials and Methods

Animals

This study was conducted in accordance with the National Institutes of Health (NIH) guidelines for the care and use of animals. The protocol was approved by the Experimental Animal Ethics Committee of the University of Tokyo (approval number: P29-11). Adult male C57BL/6 J mice (SLC) 7–11 weeks old were housed under conditions of controlled temperature and humidity (23 ± 1°C, 55 ± 5%) on a 12:12-h light/dark cycle and had access to food and water ad libitum. Mice were individually housed after surgery. All behavioral tests were performed between 8 AM and noon. Mice were acclimated by daily handling before the behavioral experiments.

Stereotaxic Surgery

Mice were anesthetized using pentobarbital (40 mg/kg, i.p.) and xylazine (10 mg/kg, i.p.) and placed in a stereotaxic apparatus. The virus cocktail (0.2–0.6 µL, University of North Carolina vector core) of adeno-associated virus (AAV)$_8$-CaMKIIα-mCherry-IRES-Cre, AAV$_5$-EF1α-DIO-ChR2(H134R)-EYFP and phosphate-buffered saline (PBS) was injected into the unilateral CA1 of the hippocampus (antero-posterior (AP): −2.0 mm, Lateral-Median (LM): ±1.6 mm, dorso-ventral (DV): −1.4 mm) at a rate of 0.1 µL/min using glass pipettes. The mice in the enhanced yellow fluorescent protein (eYFP) group were injected with a mixture of AAV$_8$-CaMKIIα-mCherry-IRES-Cre, AAV$_5$-EF1α-DIO-EYFP, and PBS. Optical fibers (200-µm core diameter, 0.48 numerical aperture; Thorlabs) epoxied to ceramic zirconia ferrules (MM-FER2007C-2300; Precision Fiber Products) were implanted unilaterally above the injection site (AP: −2.0 mm, LM: ±1.6 mm, DV: −1.2 mm). The optical fibers were secured to the skull using adhesive (LOCTITE 454; Henkel) and dental cement (Provinice; Shofu). Carbon powder was mixed with the cement to prevent light leakage. Behavioral experiments were performed 3–4 weeks after the surgery. To determine the cellular overlap of virus-infected cells and active cells during conditioning, the mice were injected with a mixture of AAV$_8$-CaMKIIα-mCherry-IRES-Cre, AAV$_9$-CAG-FLEX-tdTomato, and PBS 5 days before a fear conditioning task.

Contextual Fear Conditioning

Fear conditioning and subsequent testing were performed in a conditioning chamber (18 cm wide, 15 cm deep, and 27 cm high) that had a stainless steel grid floor. The chamber was cleaned with 70% ethanol before each session. During the conditioning session, after a 180-s acclimation period, 3 shocks (1 mA, 1 s) were delivered with a 60-s interval between shocks. The mice were kept in the chamber for an additional 60 s and then returned to their home cages. The entire duration of this session was 360 s. During the memory-retrieval test session, the animals were reexposed to the same chamber. After 60 s, 4 optical stimulations (473-nm wavelength, 20 Hz, 20 ms, 4–9 mW output from fiber) were delivered for 30 s at 30-s intervals. The stimulation frequency was chosen because 20-Hz optical stimulation has been reported to induce artificial memory retrieval and memory associations (Liu et al. 2012; Ohkawa et al. 2015). The entire duration of this session was 300 s. The mice were killed immediately after the retrieval session (experiment presented in Fig. 4A–E; *Arc* temporal activity by fluorescence in situ hybridization [catFISH] analysis) or 90 min after the conditioning session (experiment presented in Fig. 2; c-Fos immunohistochemistry). Fear memory was assessed and expressed as the percentage of time the animal remained immobile, a commonly used parameter for measuring conditioned fear in mice. Defensive immobility was defined as the absence of all movements, except those related to breathing, and automatically scored according to a previously described method using a custom-made MATLAB (R2017a; MathWorks) routine (Iwasaki et al. 2015). The instantaneous velocity in each frame was calculated based on the distance traveled during a 1-frame period of 0.5 s and was normalized by the mean of the entire session, and then a 2-s moving average was calculated.

Open-Field Test

The open-field tests were conducted in a square, white expanded box (40 cm in width, 40 cm in length). The arena of the open field included a center zone (24 cm in width and 24 cm in length). A camera was installed above the center of the field. Immediately after placement of a mouse in the center of the open field, its movement and position were recorded. After 60 s, 9 optical stimulations were delivered for 30 s at 30-s intervals. The entire duration of this session was 600 s. The time in the center zone and total distance moved were automatically calculated.

Fluorescent In Situ Hybridization

The mice were killed immediately after the memory-retrieval test session, and their brains were removed and quickly frozen. Coronal brain sections (20 µm) were prepared using a cryostat and hybridized with riboprobes (digoxigenin-*Arc* antisense riboprobe, 2 g/mL; fluorescein-channelrhodopsin2 [*ChR2*] antisense riboprobe, 2 g/mL). The signal was detected using an anti-digoxigenin alkaline phosphatase-conjugated antibody (1:1000; #11207733910; Roche, Basel, Switzerland) or an anti-fluorescein horseradish peroxidase-conjugated antibody (1:100; #11426346910; Roche) in the tyramide signal amplification (TSA) blocking buffer (PerkinElmer); a mixture of streptavidin-conjugated AlexaFluor-488 (Molecular Probes) and HNPP/FastRed (Roche) in staining buffer (100 mM Tris-Cl pH 8.0, 100 mM NaCl, 5 mM $MgCl_2$). The nuclei were counterstained with Hoechst dye (1:1000).

Immunohistochemistry

The mice were perfused with PBS followed by 4% paraformaldehyde (PFA). The brains were postfixed in 4% PFA for 4 h. The coronal sections (40 µm) were prepared using a cryostat. ChR2-eYFP was visualized with an anti-GFP primary antibody (1:500; ab13970; Abcam) and AlexaFluor-488 goat anti-chicken secondary antibody (1:500; A11039; Thermo Fisher Scientific). c-Fos was visualized with an anti-c-Fos primary antibody (1:500; sc-52; Santa Cruz Biotechnology) and biotinylated anti-rabbit secondary antibody (1:500; BA-1000; Vector Laboratories) and the TSA Plus Fluorescein System (1:100; NEL741001KT; PerkinElmer). NeuN was visualized with an anti-NeuN primary antibody (1:1000; MAB377; Merck Millipore) and AlexaFluor-594 goat anti-mouse secondary antibody (1:500; A11005; Abcam). The nuclei were counterstained with Hoechst dye (1:1000).

Confocal Microscopy and Image Analysis

Following in situ hybridization, Z-stacks of 1-μm-thick optical sections of the hippocampus (1.4–2.8 mm posterior to bregma) and basolateral amygdala (BLA) (1.2–1.4 mm posterior to bregma) were acquired using a confocal microscope (CV1000; Yokogawa Electric) at ×40 under an oil-immersion lens (NA, 1.3). Following immunohistochemistry, images of CA1 neurons were acquired using ×20 magnification under an objective lens (NA, 1.3).

Fluorescence images were analyzed using ImageJ software (NIH). The nuclei in the CA1 pyramidal layer were traced in the Hoechst channel using ImageJ software. Only cells that were presumptive neurons were included in the analysis. The total number of presumptive neurons was hand-counted in a NeuN channel of a Z-stack from each animal. This number was obtained from the volume of a single neuron, which was calculated as the density of NeuN (NeuN hand-counting/Hoechst volume). The designation of "c-Fos-positive" or "tdTomato-positive" was assigned to cells whose nuclei were entirely labeled with c-Fos or tdTomato, respectively. For the *Arc* catFISH analysis, the designation "nuclear-*Arc*-positive" was assigned to neurons that exhibited 1 or 2 of the characteristic intense intranuclear areas of fluorescence. The designation "cytoplasmic-*Arc*-positive" was assigned to neurons that contained perinuclear/cytoplasmic labeling over multiple optical sections. The reactivation index between 2 populations was obtained as follows:

$$\text{Reactivation index} = (\text{Double} - \text{chance}) / (\text{Cyto} - \text{chance}) \times 100,$$

where Double = percentage of total cytoplasmic- and nuclear-*Arc*-positive cells, chance = Cyto × Nuc/100, Cyto = percentage of total cytoplasmic-*Arc*-positive cells, and Nuc = percentage of total nuclear-*Arc*-positive cells".

To determine the number of optically induced Arc^+ cells in the CA1 pyramidal cell layer, we traced the target region (1.4–2.8 mm posterior to bregma) across 7 serial sections and determined the virus injection site. We then assessed the percentages of *ChR2*/nuclear-*Arc* double-positive cells in the CA1 pyramidal cell layer at the injection site. The total number of neurons that could theoretically be illuminated by optical stimulation was estimated based on the density of neurons in the CA1 pyramidal cell layer (Erö et al. 2018) and the putative volume of the area that could be reached by optical stimulation. Then, the estimated number of optically activated cells was obtained for each mouse by multiplying the total number of illuminated neurons by the percentages of *ChR2*/nuclear-*Arc* double-positive cells at the injection site. All analyses were conducted by an experimenter blind to the experimental conditions.

Results

Random and Sparse Activation of Unilateral CA1 Neurons

To attain sparse and nonspecific activation of hippocampal CA1 neurons, we injected an AAV cocktail, which consisted of a lower titer of AAV-CaMKIIα-Cre (AAV-Cre) and a higher titer of AAV-EF1α-DIO-ChR2-eYFP (AAV-DIO-ChR2), into the CA1 region of the mouse dorsal hippocampus (Fig. 1A). Injection of AAV-Cre aimed to express Cre in a small and randomly selected population of excitatory principal neurons, whereas injection of AAV-DIO-ChR2 aimed to express ChR2 fused to the eYFP in the Cre-positive cells. We previously demonstrated that this 2-stage method yields a large amount of Cre-dependent protein expression in a small number of cells (Nomura et al. 2015). In the brains of mice that had been treated with a mixture of AAV-Cre and AAV-DIO-ChR2, the expression of ChR2 was observed as eYFP fluorescence, which was restricted to a small region (i.e., the AAV injection site) in the dorsal CA1 region (Fig. 1B). To estimate the amount of optically evoked activity, we applied 20-ms light pulses at a wavelength of 473 nm every 50 ms (at 20 Hz) for 30 s through an optical fiber that was unilaterally implanted into the CA1 region. The mice were killed after optical stimulation, and the brains were serially sectioned and inspected using in situ hybridization for *ChR2* mRNA and *Arc* mRNA (Fig. 1C); note that *Arc*, an IEG critical for synaptic plasticity and memory, is transcribed within 5 min in a neuronal activity-dependent manner (Guzowski et al. 1999). The total number of *ChR2*-expressing cells per hippocampus ranged from 23 to 317 cells (Fig. 1D; median = 43, $n = 5$ mice), and the total number of cells that expressed both *ChR2* and *Arc* in their nuclei (nuclear-*Arc*) ranged from 10 to 178 cells (median = 33, $n = 5$ mice). *ChR2*-positive cells expressed nuclear *Arc* more frequently than *ChR2*-negative cells (Fig. 1E; $t_4 = 3.36$, $P = 2.84 \times 10^{-2}$, paired *t*-test, $n = 5$ mice), which indicated that our optical stimulation protocol preferentially activated *ChR2*-positive cells. *ChR2* was not detected in the ventral hippocampus or the hippocampus contralateral to the AAV injection site (data not shown). Therefore, we succeeded in activating a small subset of randomly selected CaMKIIα^+ cells in the CA1 pyramidal cell layer. Given that the mouse hippocampus contains approximately 440 000 neurons in the CA1 pyramidal cell layer (Erö et al. 2018), the percentage of optogenetically activated cells to the total CA1 neurons was roughly estimated to range between 0.002% and 0.04% (median = 0.008%).

We next confirmed whether Cre expression was allocated to a set of active neurons. We examined neuronal overlap between Cre-positive neurons and IEG-positive neurons during memory encoding using the mice that were cotreated with AAV-Cre and AAV-CAG-FLEX-tdTomato. To assess hippocampus-dependent memory, we employed contextual fear conditioning, a task that establishes an association between electric foot shocks and an environmental context (Phillips and LeDoux 1992). Ninety minutes after contextual fear conditioning, IEG-positive cells were detected using c-Fos immunohistostaining, whereas Cre-positive cells were visualized via the fluorescence of tdTomato (Fig. 2A,B). The ratio of tdTomato/c-Fos double-positive cells to the total cells in the AAV-injected area did not significantly differ from its stochastic chance level, which was defined as the product of the ratios of tdTomato-positive cells and c-Fos-positive cells (Fig. 2C; $t_3 = 2.43$, $P = 9.30 \times 10^{-2}$, paired *t*-test, $n = 4$ mice). Therefore, AAV infection did not affect the cell population that was activated during memory encoding, and Cre was randomly and sparsely expressed in the AAV-injected area.

Activation of Sparse CA1 Neurons Disrupts Contextual Memory Retrieval

We examined whether such a very small perturbation in CA1 activity affected memory retrieval. The mice were injected with AAVs and implanted with an optical fiber. The positions of the tips of fibers were post hoc identified (Fig. 3). The mice were

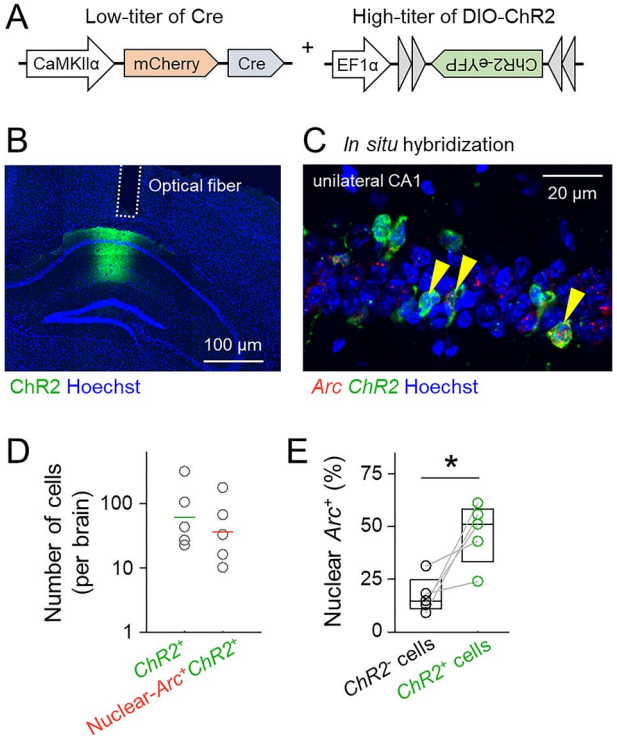

Figure 1. The dual AAV infection system allows a small subset of hippocampal CA1 cells to express ChR2. (*A*) Schematic of the virus cocktail used in this study. AAV-mCherry-Cre was injected at a low titer to express Cre sparsely in CaMKII*α*-positive cells in the hippocampal CA1 pyramidal cell layer, whereas AAV-DIO-ChR2-eYFP was injected at a high titer to express ChR2 in a large number of cells, allowing reliable firing. (*B*) Representative confocal image of ChR2-eYFP expression in the CA1 region in a coronal brain section. (*C*) Representative image of the CA1 region labeled using double FISH of *ChR2* and *Arc* immediately after optical stimulation in the hippocampus. Arrowheads indicate *ChR2*/nuclear-*Arc* double-positive cells. (*D*) Percentages of *ChR2*-positive cells (left) or *ChR2*/nuclear-*Arc* double-positive cells (right) to the total cells in the CA1 region. Horizontal lines indicate the geometric means of 5 mice. (*E*) Percentages of nuclear-*Arc*-positive cells in *ChR2*-negative cells or *ChR2*-positive cells. Nuclear-*Arc* mRNA was preferentially coexpressed with *ChR2*; $t_4 = 3.36$, $P = 2.84 \times 10^{-2}$, paired *t*-test, $n = 5$ mice.

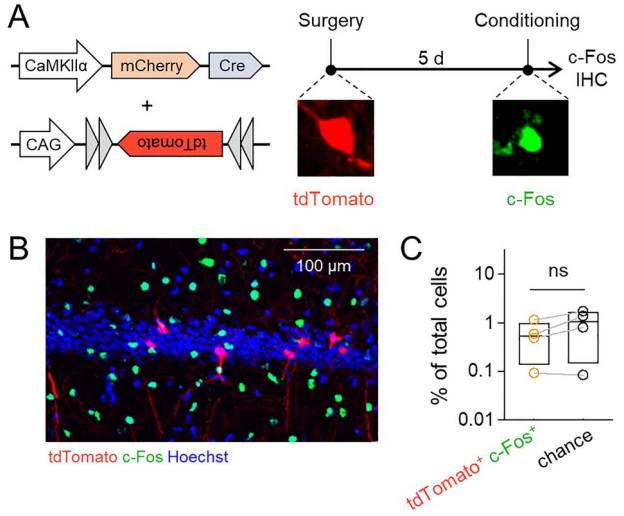

Figure 2. AAV infection does not affect neuronal allocation. (*A*) Left, virus cocktail used in this experiment. A low titer of AAV-Cre was injected for sparse expression of Cre, and a high titer of AAV-FLEX-tdTomato was injected to clearly visualize Cre-positive cells. Right, experimental schedule for this experiment. Five days after the virus injection, the mice were subjected to contextual fear conditioning and subsequently sacrificed for c-Fos immunostaining. (*B*) Representative image of tdTomato and c-Fos expression in the CA1. (*C*) The percentages of tdTomato/c-Fos double-positive cells and chance computed as the product of the probabilities of tdTomato-positive and c-Fos-positive cells; $t_3 = -2.43$, $P = 2.84 \times 10^{-2}$, paired *t*-test, $n = 4$ mice.

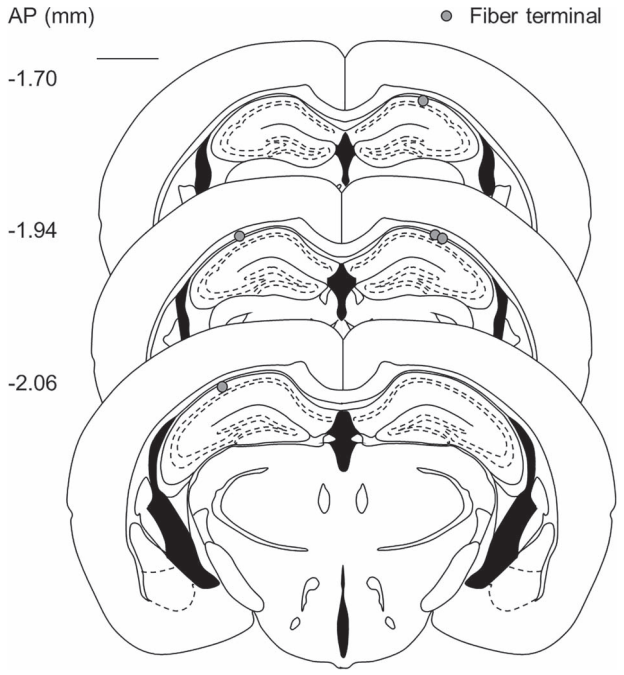

Figure 3. Locations of the tips of optical fibers are post hoc identified. Fiber locations for mice in the ChR2 group (gray circles). Scale bar = 1 mm.

divided into 2 groups, the ChR2 group and the eYFP group (Fig. 4A). The mice in the ChR2 group were unilaterally infused with AAV-Cre and AAV-DIO-ChR2 into the CA1 region, whereas the eYFP group was a control group in which mice were unilaterally infused with AAV-Cre and AAV-DIO-eYFP into the CA1 region. The mice were subjected to contextual fear conditioning 3–4 weeks after the AAV injection. After 25 min of rest in their home cages, they were placed in the same conditioning chamber for 5 min (Fig. 4A). In this memory-retrieval session, optical stimulation with 20-ms light pulses at a wavelength of 473 nm at 20 Hz for 30 s was repeated every 60 s (Fig. 4B). Contextual memory was assessed as the percentage of time spent in defensive immobility in the conditioned context. Immediately after the onset of optical stimulation, the instantaneous velocity quickly increased and remained high as long as the optical stimulation persisted (Fig. 4B,C). Thus, light delivery decreased immobility. On average, without optical stimulation (baseline period), the mice showed high defensive immobility, but with optical stimulation (ON period), immobility was decreased in the ChR2 group (Fig. 2D; $t_4 = 4.76$, $P = 8.93 \times 10^{-3}$, paired *t*-test, $n = 5$ mice). The immobility time of the mice in the eYFP group was not affected by optical stimulation (Fig. 4E; $t_4 = 0.19$, $P = 0.856$, paired *t*-test, $n = 5$ mice).

We next examined whether the effect of optical stimulation arose from altered locomotion or anxiety rather than memory-retrieval failure. The mice in the ChR2 group were subjected

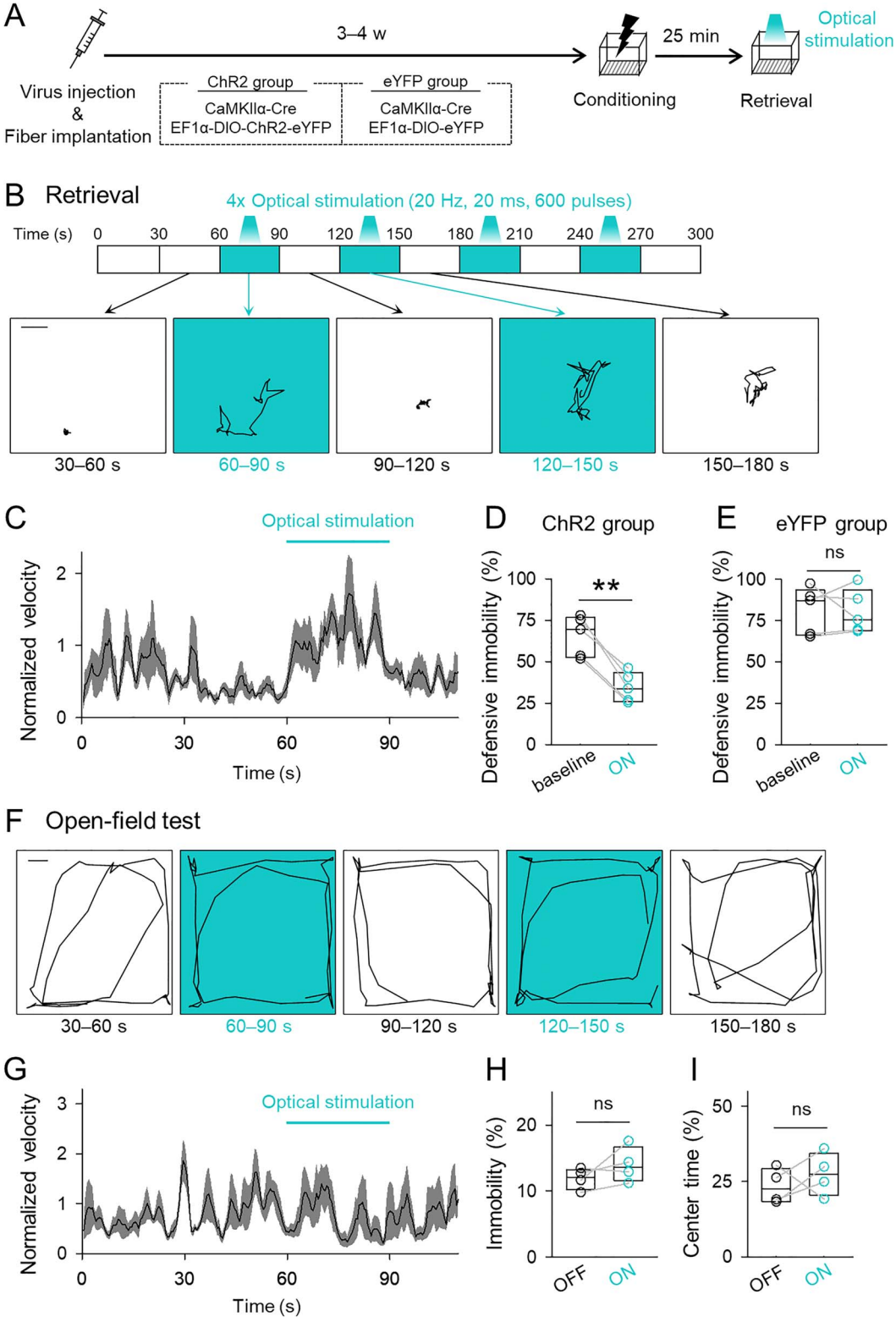

Figure 4. Optogenetic activation of a small subset of CA1 cells disrupts memory retrieval but does not affect locomotor activity or anxiety. (*A*) Experimental paradigm. Mice that had been administered a mixture of AAVs and implanted with an optical fiber into the unilateral CA1 were subjected to contextual fear conditioning and reexposure to the conditioned context for memory retrieval. In the retrieval session, optical stimulation was intermittently delivered. (*B*) Top, time courses of optical stimulation in the retrieval session. Bottom, representative traces of the location of a mouse during each 30-s period in the retrieval session. Scale bar = 3 cm. (*C*) The 2-s moving average of the instantaneous velocity of the ChR2 group during the retrieval session. The velocities were normalized by the mean of the entire session.

to an open-field test with or without optical stimulation. The same optical stimulation did not affect the percentages of immobility time in the open arena (Fig. 4F–H; $t_3 = 1.53$, $P = 0.224$, paired t-test, $n = 4$ mice) or time spent in the center of the arena, a measure of anxiety (Fig. 4I; $t_3 = 2.75 \times 10^{-2}$, $P = 0.980$, paired t-test, $n = 4$ mice). These results suggested that our optical activation induced transient and reversible amnesia without affecting spontaneous locomotor activity or anxiety.

Activation of Sparse CA1 Neurons Fails to Affect Hippocampal Reactivation

We sought to determine the mechanisms underlying optogenetically induced amnesia. Reactivation of an ensemble of IEG-positive cells that were activated during memory encoding is essential for memory recall (Tonegawa et al. 2015). The hippocampus is critical to drive contextual emotional memory and reinstatement of cortical memory representations (Liu et al. 2012; Tanaka et al. 2014; Trouche et al. 2016). Thus, we hypothesized that our optogenetic CA1 stimulation disrupted neuronal reactivation of hippocampal IEG-positive cells. To assess this hypothesis, we simultaneously visualized *Arc*-positive cell ensembles that were activated during memory encoding and/or memory retrieval using cellular compartment analysis of catFISH (Guzowski et al. 1999; Sakaguchi et al. 2018). Because *Arc* mRNA accumulates in the neuronal nuclei within 5 min and in the cytoplasm 20–45 min after neuronal activity (Guzowski et al. 1999), neurons that had been active during contextual fear conditioning and memory retrieval were detected as cytoplasmic-*Arc*-positive cells and nuclear-*Arc*-positive cells, respectively, when *Arc* mRNA was visualized immediately after the memory-retrieval session (Fig. 5A,B). We indeed observed cytoplasmic and nuclear *Arc*-positive cells in the hippocampal CA1 pyramidal cell layer, whose percentages to the total cells were consistent with previously reported values (Pevzner and Guzowski 2014; Sakaguchi et al. 2018). Interestingly, the percentages of cytoplasmic and nuclear *Arc*-positive cells did not differ between the ChR2 group and the eYFP group (Fig. 5D; cytoplasmic: $t_8 = 1.52$, $P = 0.168$ (Fig. 3E); nuclear: $t_8 = 0.316$, $P = 0.760$; Student's t-test, $n = 5$ mice each), indicating that optogenetically induced memory disruption was not caused by a change in the overall activity level of CA1 neurons. The ChR2 group did not show an increase in the number of nuclear-*Arc*-positive cells even in the presence of the additional small amount of activity by optical stimulation, which may have been because the additional noise was too small to statistically affect the percentages of *Arc*-positive cells. We next computed the ratio of reactivated neurons (reactivation index), which was calculated by dividing the number of cytoplasmic/nuclear double-*Arc*-positive cells by the number of cytoplasmic-*Arc*-positive cells. The reactivation index did not differ between the ChR2 group and the eYFP group (Fig. 5F; $t_8 = 0.864$, $P = 0.413$, Student's t-test, $n = 5$ mice each). To confirm that ChR2 expression did not affect *Arc* expression, we analyzed the neuronal overlap ratios between cytoplasmic-*Arc*-positive cells and *ChR2*-positive cells. The percentages of cytoplasmic-*Arc*/*ChR2* double-positive cells did not significantly differ from the stochastic chance level (Fig. 5G; $t_4 = 1.75$, $P = 0.155$, paired t-test, $n = 5$ mice). Therefore, ChR2 expression did not affect the patterns of *Arc* expression, in a manner similar to c-Fos expression (Fig. 2). Moreover, optogenetically induced changes in defensive immobility time were not correlated with the reactivation index or the percentages of nuclear-*Arc*-positive cells (Fig. 5H,I). These results indicated that optogenetically activated CA1 neurons were too sparse to affect the CA1 reactivation patterns as a whole. Furthermore, the percentage of nuclear-*Arc*/*ChR2* double-positive cells, that is, the population of optogenetically activated cells, was not correlated with optogenetically induced memory impairment (Fig. 5J), suggesting that memory retrieval was disrupted only when the amount of noisy activity exceeded a certain threshold and that the amount of noise did not determine the degree of memory impairment in a graded manner.

Activation of Sparse CA1 Neurons Disrupts Amygdalar Reactivation

The amygdalar complex, especially the BLA, is involved in contextual aversive memories (LeDoux 2000; Girardeau et al. 2017). The BLA serves to associate neutral contexts with aversive stimuli and is essential for the retrieval of contextual fear memory (Janak and Tye 2015). We repeated the same *Arc* catFISH analysis for BLA neurons. As in the CA1 region, we found that the activity percentages were consistent with previously reported values (Yokose et al. 2017; Sakaguchi et al. 2018) and that the percentages of cytoplasmic- or nuclear-*Arc*-positive BLA cells did not significantly differ between the ChR2 group and the eYFP group (Fig. 6B; cytoplasmic: $t_8 = 0.450$, $P = 0.665$ (Fig. 6C); nuclear: $t_8 = 0.826$, $P = 0.433$; Student's t-test, $n = 5$ mice each). However, the reactivation index was lower in the ChR2 group than in the eYFP group (Fig. 6D; $t_8 = 3.50$, $P = 8.14 \times 10^{-3}$, Student's t-test, $n = 5$ mice each). Optogenetically induced changes in defensive immobility time were positively correlated with the reactivation index (Fig. 6E) but not with the percentage of nuclear-*Arc*-positive cells (Fig. 6F). Moreover, the percentage of nuclear-*Arc*/*ChR2* double-positive cells in the CA1 did not correlate with the reactivation index (Fig. 6G). These data indicated that optogenetic sparse activation of CA1 neurons altered the reactivation pattern, but not the overall activity level, of *Arc*-positive cells in the BLA, suggesting that the addition of a small amount of noise into the CA1 network disrupted contextual representation in the hippocampus that differentially activated downstream BLA neurons.

Discussion

In this study, we optogenetically activated a randomly selected approximately 0.008% of hippocampal cells in the CA1 pyramidal cell layer during memory retrieval in a contextual fear

The black line and the gray areas indicate means ± SEMs. (*D*) The mean percentages of time spent in behavioral defensive immobility were compared between periods before the light delivery (baseline) and during the light-ON epoch in the ChR2 group; $t_4 = 4.76$, $P = 8.93 \times 10^{-3}$, paired t-test, $n = 5$ mice. (*E*) The mean percentage of defensive immobility time in the eYFP group; $t_4 = 0.193$, $P = 0.856$, paired t-test, $n = 5$ mice. (*F*) Representative traces of the location of a mouse during each 30-s period in the open-field test. Scale = 10 cm. (*G*) The 2-s moving average of normalized instantaneous velocity during the open-field test. The black line and the gray areas indicate means ± SEMs. (*H*) The time in immobility with or without optical stimulation in the open-field test; $t_3 = 1.53$, $P = 0.224$, paired t-test, $n = 4$ mice. (*I*) The mean percentages of the time spent in the center zone; $t_3 = -2.75 \times 10^{-2}$, $P = 0.980$, paired t-test, $n = 4$ mice.

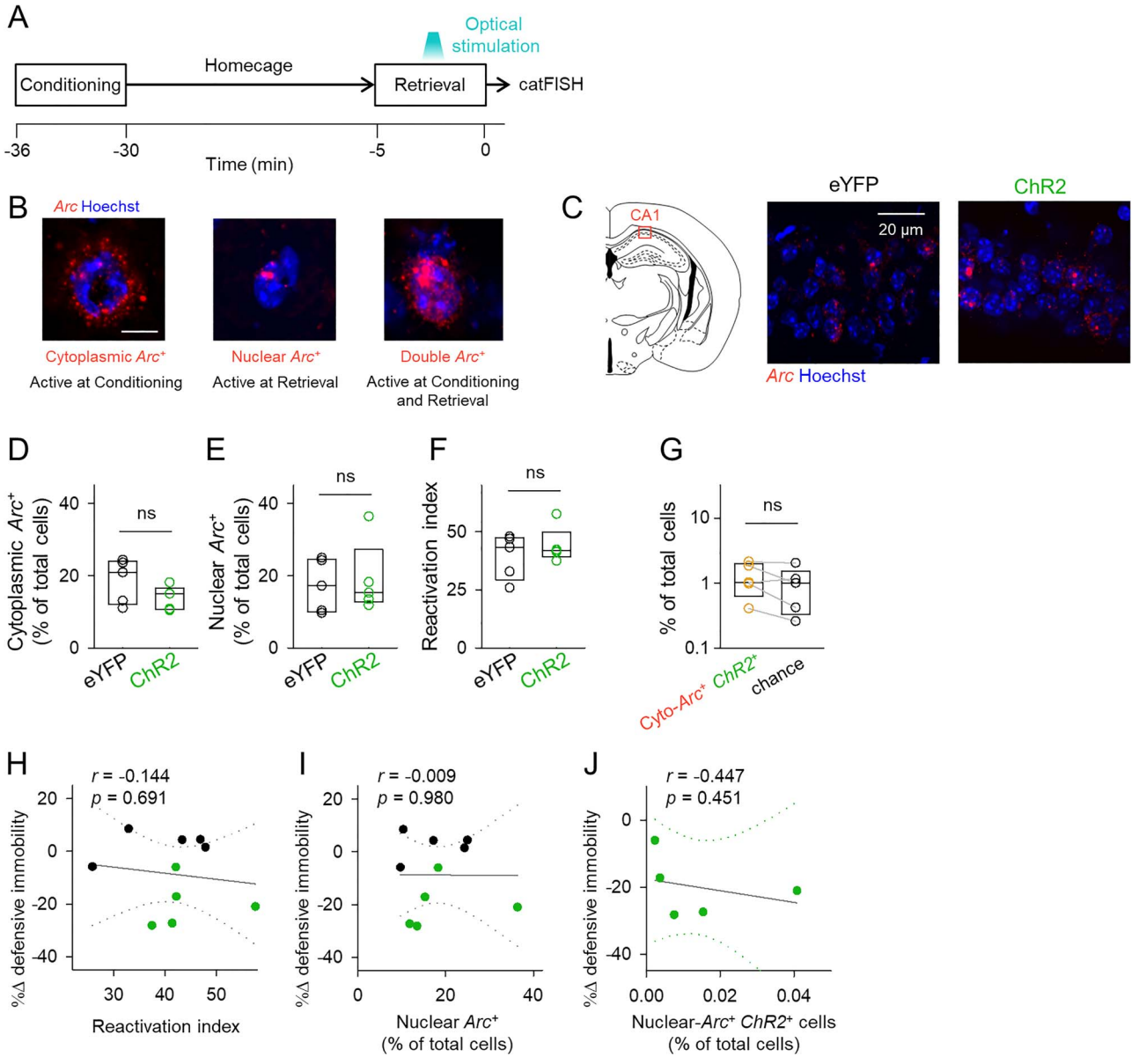

Figure 5. Optogenetic activation of a small subset of CA1 cells does not affect the activation pattern in the CA1. (*A*) Experimental paradigm for the *Arc* catFISH experiment. After contextual fear conditioning, the mice stayed in their home cage for 25 min. Immediately, after the retrieval session, the mice were sacrificed and processed for in situ hybridization for *Arc*. (*B*) The time courses of *Arc* RNA expression. Transcribed *Arc* first appears in neuronal nuclei and processed *Arc* then accumulates in the cytoplasm. Therefore, the cytoplasmic-*Arc*-positive cells and the nuclear-*Arc*-positive cells were estimated to be active cells during conditioning and retrieval sessions, respectively. (*C*) Left, illustration of the region analyzed in the catFISH experiment. Right, representative images of *Arc* in the CA1. (*D, E*) The percentages of cytoplasmic-*Arc*-positive cells (left) and nuclear *Arc*-positive cells (*right*). Cytoplasmic: $t_8 = 1.52$, $P = 0.168$; nuclear: $t_8 = -0.316$, $P = 0.760$; Student's *t*-test, $n = 5$ mice each. (*F*) The ratio of reactivated cytoplasmic-*Arc*-positive cells (i.e., reactivation index); $t_8 = 0.864$, $P = 0.413$, Student's *t*-test, $n = 5$ mice each. (*G*) The percentages of cytoplasmic-*Arc*/*ChR2* double-positive cells and their chance levels that were computed as the product of the probabilities of cytoplasmic-*Arc*-positive and *ChR2*-positive cells; $t_4 = 1.75$, $P = 0.155$, paired *t*-test, $n = 5$ mice. (*H–J*) Correlation plots of optical stimulation-induced changes in the defensive immobility time (light ON—before) during the retrieval session against the reactivation index (*H*), the percentages of nuclear-*Arc*-positive cells (*I*), and the percentages of nuclear-*Arc*/*ChR2* double-positive cells. Dotted lines indicate 95% confidence intervals.

conditioning paradigm. We found that this very small level of CA1 perturbation was enough to disrupt the reactivation pattern in BLA neurons and prevent fear memory retrieval. These results suggest that the hippocampal representation of the environmental context is so tightly regulated that memory retrieval is vulnerable to unnecessary neuronal activity. Therefore, during contextual fear memory retrieval, the hippocampus not only activates memory engram cells but also actively silences memory-irrelevant cells.

To investigate the mechanisms for optogenetically disrupted memory retrieval, we visualized *Arc*-positive cells in the hippocampus during memory encoding and retrieval. We assumed that sparse activation of hippocampal neurons perturbed the reactivation of CA1 *Arc*-positive cells because, in general, the

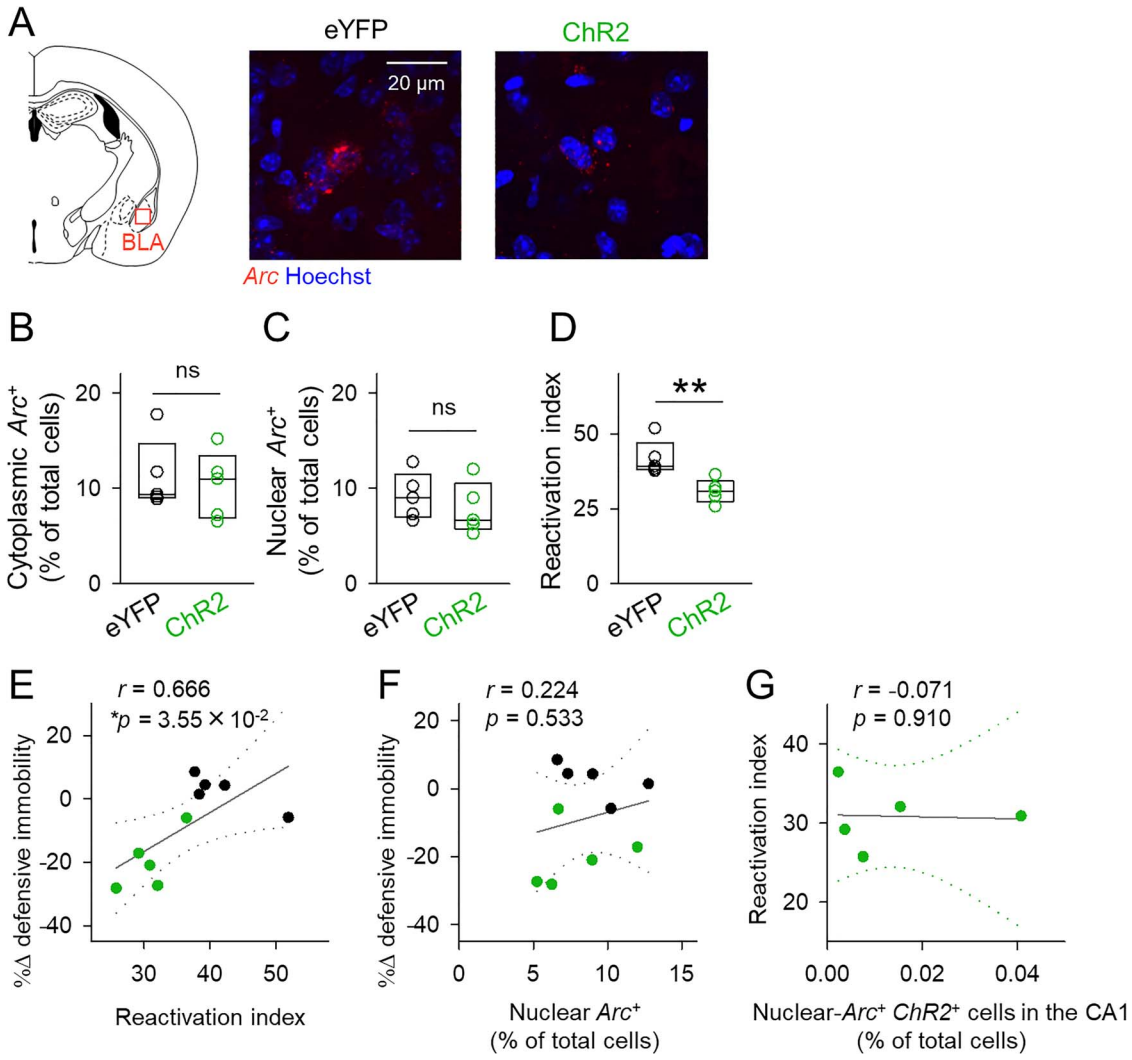

Figure 6. Optogenetic activation of a small subset of CA1 cells disrupts reactivation of BLA neurons. (*A*) Left, illustration of the region analyzed in the catFISH experiment. Right, representative images of *Arc* in the BLA. (*B*, *C*) The percentages of cytoplasmic-*Arc*-positive cells (left) and nuclear-*Arc*-positive cells (right). Cytoplasmic: $t_8 = 0.450$, $P = 0.665$; nuclear: $t_8 = 0.826$, $P = 0.433$; Student's *t*-test, $n = 5$ mice each. (*D*) The ratio of reactivated cytoplasmic-*Arc*-positive cells (i.e., reactivation index); $t_8 = 3.50$, $P = 8.14 \times 10^{-3}$, Student's *t*-test, $n = 5$ mice each. (*E*, *F*) Correlation plots of optical stimulation-induced changes in the defensive immobility time (light ON—before) during the retrieval session against the reactivation index (*E*) and the percentages of nuclear-*Arc*-positive cells (*F*). (*G*) Correlation plot of the reactivation index against the percentages of nuclear-*Arc*/*ChR2* double-positive cells. Dotted lines indicate 95% confidence intervals.

activity of a neuron affects other neurons. There are also mutually inhibitory circuits in the hippocampus that regulate the size of active cell ensembles (Freund and Buzsáki 1996; Sun et al. 2014; Stefanelli et al. 2016). Therefore, externally elicited activity in some neurons propagates to other neurons and changes the entire activity pattern in the neuronal network. Consistent with this idea, optogenetic inhibition of a *c-Fos*-tagged CA1 neuron subset induced the alternative activation of another neuron ensemble (Tanaka et al. 2014; Trouche et al. 2016). Thus, we expected that artificial activation of a CA1 cell subset collapsed memory representations because the activity of other CA1 neurons was modified. However, we failed to find that sparse activation of CA1 neurons affected the overall global Arc-positive patterns in the CA1 region. Most likely, our neuronal perturbation was too weak to be detected in the population analysis.

Previous studies have suggested that reactivation of IEG-tagged hippocampal cells during memory acquisition was essential for retrieval of contextual emotional memory (Denny et al. 2014; Tanaka et al. 2014; Park et al. 2016; Trouche et al. 2016). We also confirmed that CA1 neuronal reactivation occurred even under optogenetic activation of CA1 neurons, but memory retrieval was impaired at the behavioral level. These results indicated that reactivation of IEG-tagged neurons alone cannot account for successful memory recall. Rather, the small activity perturbation was likely to alter the hippocampal representation of the environmental context and alter active cell ensembles in downstream networks, such as in the BLA, a brain region required to express fear memory recall. Therefore, we conclude that memory retrieval depends on the highly precise reactivation of IEG-positive cells and, thus, is vulnerable to additional CA1 noise.

Because small amounts of optogenetic activation inhibited reactivation in the BLA, other types of amygdala-dependent memories, for example, cued fear conditioning or conditioned

taste aversion, may also be interfered with by hippocampal noise. In addition, inhibition of hippocampal engram cells disrupts reactivation in various cortical regions, including the perirhinal cortex, retrosplenial cortex, and entorhinal cortex (Tanaka et al. 2014), suggesting that abnormal hippocampal activity may alter active cell ensembles even in other brain regions. Therefore, our protocol to induce small amounts of activity in the hippocampus may affect not only contextual fear conditioning but also other tasks that are not dependent on the BLA.

Although the effects of random activation of CA1 cells had not been elucidated, it is known that artificial activation of a different set of memory engram cells interferes with memory recall. For example, contextual fear memory was disrupted by chemogenetic activation of memory engram cells that encoded a different context that was not associated with any valence (Garner et al. 2012; Poll et al. 2020). In these studies, the different cell ensembles were captured using *c-Fos* to tag another memory engram, but not a nonmemory engram, which was thereafter activated. On the other hand, we introduced ChR2 into a small number of cells under the CaMKIIα promoter in a randomly selected manner. We believe that our study is the first to demonstrate that random activation of CA1 nonmemory engram cells disrupts neuronal reactivation and memory recall.

Animal models of AD display disruptions in memory retrieval but not memory acquisition (Roy et al. 2016). They also exhibit an increase in abnormally hyperactive neurons in the hippocampus (Busche et al. 2012). Human imaging studies have also revealed elevated hippocampal activity in patients with early AD or amnestic mild cognitive impairment (Dickerson et al. 2005; Celone et al. 2006; O'Brien et al. 2010). A recent study suggested that memory retrieval failure in AD-like conditions was attributable to the presence of extraneuronal activity in the CA1 region (Poll et al. 2020); inactivation of extraneuronal activity rescued memory disruption in a mouse model of early AD, suggesting that reducing noisy activity contributes to improvements in memory retrieval under pathological conditions. Although abnormally elevated activity is thought to disturb coordinated neuronal activity and lead to impairments in memory recall, there is no direct evidence for the causal relationship between hippocampal hyperactivity and amnesia. In the context of these findings, it was intriguing to find our results showing that sparse CA1 hyperactivation disrupted memory retrieval in the contextual fear conditioning paradigm. Our work will contribute to understanding the mechanisms underlying memory recall as well as the role of hyperactivity of CA1 neurons in amnesia.

Notes

Conflict of Interest: None declared.

Funding

The Japan Science and Technology Agency, Exploratory Research for Advanced Technology (JPMJER1801 to Y.I.); Japan Society for the Promotion of Science, Grants-in-Aid for Scientific Research (18H05525 to Y.I.).

References

Busche MA, Chen X, Henning HA, Reichwald J, Staufenbiel M, Sakmann B, Konnerth A. 2012. Critical role of soluble amyloid-β for early hippocampal hyperactivity in a mouse model of Alzheimer's disease. *Proc Natl Acad Sci U S A*. 109:8740–8745.

Celone KA, Calhoun VD, Dickerson BC, Atri A, Chua EF, Miller SL, DePeau K, Rentz DM, Selkoe DJ, Blacker D, et al. 2006. Alterations in memory networks in mild cognitive impairment and Alzheimer's disease: an independent component analysis. *J Neurosci*. 26:10222–10231.

Cowansage KK, Shuman T, Dillingham BC, Chang A, Golshani P, Mayford M. 2014. Direct reactivation of a coherent neocortical memory of context. *Neuron*. 84:432–441.

Denny CA, Kheirbek MA, Alba EL, Tanaka KF, Brachman RA, Laughman KB, Tomm NK, Turi GF, Losonczy A, Hen R. 2014. Hippocampal memory traces are differentially modulated by experience, time, and adult neurogenesis. *Neuron*. 83:189–201.

Dickerson BC, Salat DH, Greve DN, Chua EF, Rand-Giovannetti E, Rentz DM, Bertram L, Mullin K, Tanzi RE, Blacker D, et al. 2005. Increased hippocampal activation in mild cognitive impairment compared to normal aging and AD. *Neurology*. 65:404–411.

Erö C, Gewaltig MO, Keller D, Markram H. 2018. A cell atlas for the mouse brain. *Front Neuroinform*. 12:84.

Freund TF, Buzsáki G. 1996. Interneurons of the hippocampus. *Hippocampus*. 6:347–470.

Garner AR, Rowland DC, Hwang SY, Baumgaertel K, Roth BL, Kentros C, Mayford M. 2012. Generation of a synthetic memory trace. *Science*. 335:1513–1516.

Girardeau G, Inema I, Buzsáki G. 2017. Reactivations of emotional memory in the hippocampus-amygdala system during sleep. *Nat Neurosci*. 20:1634–1642.

Guzowski JF, McNaughton BL, Barnes CA, Worley PF. 1999. Environment-specific expression of the immediate-early gene Arc in hippocampal neuronal ensembles. *Nat Neurosci*. 2:1120–1124.

Han JH, Kushner SA, Yiu AP, Hsiang HL, Buch T, Waisman A, Bontempi B, Neve RL, Frankland PW, Josselyn SA. 2009. Selective erasure of a fear memory. *Science*. 323:1492–1496.

Iwasaki S, Sakaguchi T, Ikegaya Y. 2015. Brief fear preexposure facilitates subsequent fear conditioning. *Neurosci Res*. 95:66–73.

Janak PH, Tye KM. 2015. From circuits to behaviour in the amygdala. *Nature*. 517:284–292.

Kitamura T, Ogawa SK, Roy DS, Okuyama T, Morrissey MD, Smith LM, Redondo RL, Tonegawa S. 2017. Engrams and circuits crucial for systems consolidation of a memory. *Science*. 356:73–78.

LeDoux JE. 2000. Emotion circuits in the brain. *Annu Rev Neurosci*. 23:155–184.

Liu X, Ramirez S, Pang PT, Puryear CB, Govindarajan A, Deisseroth K, Tonegawa S. 2012. Optogenetic stimulation of a hippocampal engram activates fear memory recall. *Nature*. 484:381–385.

Nomura H, Hara K, Abe R, Hitora-Imamura N, Nakayama R, Sasaki T, Matsuki N, Ikegaya Y. 2015. Memory formation and retrieval of neuronal silencing in the auditory cortex. *Proc Natl Acad Sci U S A*. 112:9740–9744.

Nonaka A, Toyoda T, Miura Y, Hitora-Imamura N, Naka M, Eguchi M, Yamaguchi S, Ikegaya Y, Matsuki N, Nomura H. 2014. Synaptic plasticity associated with a memory engram in the basolateral amygdala. *J Neurosci*. 34:9305–9309.

O'Brien JL, O'Keefe KM, LaViolette PS, DeLuca AN, Blacker D, Dickerson BC, Sperling RA. 2010. Longitudinal fMRI in elderly reveals loss of hippocampal activation with clinical decline. *Neurology*. 74:1969–1976.

Ohkawa N, Saitoh Y, Suzuki A, Tsujimura S, Murayama E, Kosugi S, Nishizono H, Matsuo M, Takahashi Y, Nagase M, et al. 2015. Artificial association of pre-stored information to generate a qualitatively new memory. *Cell Rep*. 11:261–269.

Park S, Kramer EE, Mercaldo V, Rashid AJ, Insel N, Frankland PW, Josselyn SA. 2016. Neuronal allocation to a hippocampal engram. *Neuropsychopharmacology*. 41:2987–2993.

Pevzner A, Guzowski JF. 2014. Immediate-early gene transcriptional activation in hippocampus CA1 and CA3 does not accurately reflect rapid, pattern completion-based retrieval of context memory. *Learn Mem*. 22:1–5.

Phillips RG, LeDoux JE. 1992. Differential contribution of amygdala and hippocampus to cued and contextual fear conditioning. *Behav Neurosci*. 106:274–285.

Poll S, Mittag M, Musacchio F, Justus LC, Giovannetti EA, Steffen J, Wagner J, Zohren L, Schoch S, Schmidt B, et al. 2020. Memory trace interference impairs recall in a mouse model of Alzheimer's disease. *Nat Neurosci*.

Reijmers LG, Perkins BL, Matsuo N, Mayford M. 2007. Localization of a stable neural correlate of associative memory. *Science*. 317:1230–1233.

Roy DS, Arons A, Mitchell TI, Pignatelli M, Ryan TJ, Tonegawa S. 2016. Memory retrieval by activating engram cells in mouse models of early Alzheimer's disease. *Nature*. 531: 508–512.

Sakaguchi T, Iwasaki S, Okada M, Okamoto K, Ikegaya Y. 2018. Ethanol facilitates socially evoked memory recall in mice by recruiting pain-sensitive anterior cingulate cortical neurons. *Nat Commun*. 9:3526.

Stefanelli T, Bertollini C, Lüscher C, Muller D, Mendez P. 2016. Hippocampal somatostatin interneurons control the size of neuronal memory ensembles. *Neuron*. 89:1074–1085.

Sun Y, Nguyen AQ, Nguyen JP, Le L, Saur D, Choi J, Callaway EM, Xu X. 2014. Cell-type-specific circuit connectivity of hippocampal CA1 revealed through Cre-dependent rabies tracing. *Cell Rep*. 7:269–280.

Tanaka KZ, Pevzner A, Hamidi AB, Nakazawa Y, Graham J, Wiltgen BJ. 2014. Cortical representations are reinstated by the hippocampus during memory retrieval. *Neuron*. 84:347–354.

Tonegawa S, Liu X, Ramirez S, Redondo R. 2015. Memory engram cells have come of age. *Neuron*. 87:918–931.

Trouche S, Perestenko PV, van de Ven GM, Bratley CT, McNamara CG, Campo-Urriza N, Black SL, Reijmers LG, Dupret D. 2016. Recoding a cocaine-place memory engram to a neutral engram in the hippocampus. *Nat Neurosci*. 19:564–567.

Yokose J, Okubo-Suzuki R, Nomoto M, Ohkawa N, Nishizono H, Suzuki A, Matsuo M, Tsujimura S, Takahashi Y, Nagase M, et al. 2017. Overlapping memory trace indispensable for linking, but not recalling, individual memories. *Science*. 355:398–403.